



Transport and Fate of Ureolytic *Sporosarcina pasteurii* in Saturated Sand Columns: Experiments and Modelling

Guijie Sang¹ · Rebecca J. Lunn¹ · Grainne El Mountassir¹ · James M. Minto¹

Received: 27 January 2023 / Accepted: 13 June 2023 / Published online: 28 June 2023
© The Author(s) 2023

Abstract Despite a broad application of ureolytic bacteria in many bioremediation and biocementation processes, very limited studies have reported their transport and retention behaviors under various physical–chemical–biological conditions. In this study, we report transport and retention of *Sporosarcina pasteurii* in saturated sand, based on a series of column breakthrough experiments under different conditions including ionic strengths (ISs: 0.5 mM–1 M), flow velocity (50, 100, 200 cm/h), bacteria optical density ($OD_{600}=1.0, 0.48$), column length (280 mm, 150 mm), and changes in IS conditions (0.5 M $CaCl_2$ or deionised water). We use a two-site kinetic model, representing (1) attachment on grain surfaces, and (2) straining at crevices and constrictions, to quantify and predict the bacterial attachment and straining. Model parameters were calibrated by tracer (NaCl) breakthrough curves (BTCs) and bacteria BTCs at different IS/velocity conditions. The model was then applied to successfully predict the bacteria BTCs at lower initial bacteria density ($OD_{600}=0.48$) and for shorter column lengths (150 mm). We demonstrated that higher ionic strength (from 0.5 to 1000 mM) dramatically enhanced the retention efficiency of *S. pasteurii* through an enhancement of attachment (from 9.4 to 69.6%) and straining (from 8.1 to 34.2%), whilst the bacterial survival and the urease activity were unaffected at high IS conditions (500 and 1000 mM NaCl) within 5 h. Increasing flow velocity (from 50 to 200 cm/h) caused a decrease in attachment (from 39.5 to 22.4%) and decrease in straining (from 40.5 to 19.3%) as a result of the increased hydrodynamic shear forces, which tends to reduce the attachment at the secondary minimum and decrease the extent of flow stagnation regions for straining. Lower initial bacteria OD_{600} (from 1.0 to 0.48) enhanced the attachment (from 31.8 to 40.9%) and the straining (from 22.9 to 42.2%) as a result of reducing the site-blockage effect. In addition, 0.5 M $CaCl_2$ with a stronger IS increased the retention of in the column, whilst deionised water with a lower IS caused bacterial release. These findings provide useful information for a better understanding of the transport and fate of *Sporosarcina pasteurii* in saturated soil, and can be used to optimise bioaugmentation strategy and cementation efficiency for soil improvement.

Article Highlights

- Transport of *S. pasteurii* in sands is highly affected by ionic strength, flow velocity, bacteria density, and even column size
- Straining was enhanced (from 8.1% to 34.2%) if increasing IS (from 0.5 to 500 mM) without affecting bacterial survival

Extended author information available on the last page of the article

- Bacteria coagulation among 2–3 bacterial cells occurs under ISs of 500 and 1000 mM without forming large flocculation

Keywords Attachment · Pore straining · Ionic strength · Flow velocity · Bioaugmentation · Bacterial survival

1 Introduction

Microbially induced calcium carbonate precipitation (MICP) is an environmentally sustainable bio-remediation process that has been widely studied for a range of geo-environmental and geotechnical applications including co-precipitation of metal contaminants or radionuclides (Fujita et al. 2008; Lauchnor et al. 2013), carbon capture and storage (Minto et al. 2017; Mitchell et al. 2010), rock fracture sealing/strengthening (Minto et al. 2016; Phillips et al. 2016; Tobler et al. 2018) and soil improvement (DeJong et al. 2010; Gomez et al. 2015; El Mountassir et al. 2018; Whiffin et al. 2007). One of the most extensively utilised microorganisms for MICP is *Sporosarcina pasteurii* (*S. pasteurii*) which, via the production of the urease enzyme, catalyses the hydrolysis of urea to carbonate and ammonia, resulting in an increase in pH and precipitation of calcium carbonate if calcium is available (Stocks-Fischer et al. 1999). The precipitation of calcium carbonate can act to immobilise contaminants, reduce permeability of porous/fractured media, and improve the hydromechanical properties of soils and/or fractured rocks by bonding solid grains and bridging across surfaces (e.g. increasing shear strength, stiffness, elastic velocity) (Cuthbert et al. 2013; Minto et al. 2016, 2018; El Mountassir et al. 2014).

Bioremediation processes of MICP for soil improvement involves either a bioaugmentation or a biostimulation scheme, or a combination of both (Burbank et al. 2013; Gomez et al. 2017; Jiang et al. 2022). Major advantages of bioaugmentation schemes include faster and higher treatment efficiency. Despite the viability of bioaugmentation having been demonstrated at both laboratory and field scale (Gomez et al. 2015; Martinez et al. 2013; Nassar et al. 2018; van Paassen et al. 2010; Phillips et al. 2016; Salifu et al. 2016), it remains challenging to optimise treatment strategies so as to achieve an effective and even distribution of MICP along the flow direction. Field bioaugmentation treatment strategies involve the injection of multiple fluids: bacterial suspension (e.g. *S. pasteurii*), cementing solution (composed of urea and calcium chloride as a minimum), and injection of water pulses to minimise precipitation within injection lines and clogging around the well (Minto et al. 2019). Indeed, bioaugmentation may involve many repeated cycles of injection of some, or all, of these fluids. As such, a variety of chemical and physical perturbations are introduced after bacterial injection, such as changes in pore solution chemistry due to injection of the cementing solution (calcium chloride and urea), and due to injection of water pulses to prevent clogging. In addition, the injection of bacteria in porous/fractured media involves a non-uniform distribution of flow velocity, potentially causing spatial differences in attachment/detachment behavior due to variations in the hydrodynamic forces (Camesano and Logan 1998; Hendry et al. 1999). A fundamental understanding of the transport and fate of *S. pasteurii* in porous/fractured media under various controlling factors (e.g. ionic strength, chemical perturbation, flow velocity) is key to achieving an effective delivery of bacteria in bioaugmentation schemes and hence to achieving more efficient and economical MICP applications (Hommel et al. 2016; Kwak et al. 2023).

Two main bacteria retention phenomena are known to occur; physicochemical deposition (attachment) and straining. Colloid filtration theory (Yao et al. 1971) is widely used to predict retention of particles in suspension, but may not be adequate for predicting bacterial attachment and straining (Bradford et al. 2006; Foppen et al. 2007) due to the bacteria-specific cell characteristics (Liu et al. 2011; Stumpp et al. 2011). Predicting bacterial attachment and straining in natural porous media is considered challenging (Hommel et al. 2016) as both may be influenced by factors such as fluid chemistry (Harvey et al. 2010; Kinoshita et al. 1993; Redman et al. 2004; Torkezaban et al. 2008b), pore velocity (Camesano and Logan 1998; Choi et al. 2007), temperature (McCaulou et al. 1995), surface roughness (Shellenberger and Logan 2002), and grain size (Bai et al. 2016; Gargiulo et al. 2007). Bradford et al. (2013) reviewed the transport and fate of microbial pathogens in agricultural settings and summarised the literature on one- or two-site kinetic models for quantifying attachment and straining of bacteria or colloids based on the HYDRUS-1D software package (Bradford et al. 2006, 2003; Foppen et al. 2007; Simunek et al. 2005; Šimunek et al. 1999, 2006; Torkezaban et al. 2008a). They noted that each study advanced the understanding of attachment and pore straining phenomena under relevant physical and chemical conditions. However, bacterial transport and fate is known to vary with bacterial strain and is highly dependent on cell surface composition (Rijnaarts et al. 1996; Walker et al. 2004), cell motility (Creppy et al. 2019; Liu et al. 2011), cell size and shape (Li and Ma 2018; Seymour et al. 2013; Weiss et al. 1995), and even growth stage (Walker et al. 2005). To date, very limited studies have been systematically conducted on investigation of the transport behavior of *S. pasteurii*, which may behave differently to other bacteria and colloids. Tobler et al. (2014) investigated *S. pasteurii* transport within sandstone cores for two flow rates, two different bacteria densities and three rock core lengths. Jain and Arnepalli (2020) studied attachment and detachment of ureolytic bacteria on sands under a range of ionic strengths (0–100 mM). However, to underpin the optimization of bioaugmentation schemes for engineering soil improvement, there remains a need to understand and predict the transport and fate of *S. pasteurii* under a broad range of ionic strengths, with varying flow velocities and bacterial concentrations (Minto et al. 2019; van Wijngaarden et al. 2016, 2011). In particular, research has shown that the increase in soil strength via calcite precipitation is mainly determined by the formation of calcite bridges between grain contacts, rather than by the coating of grain surfaces with calcite (Ismail et al. 2002; Tang et al. 2020; Xiao et al. 2019). To this end, maximising straining of *S. pasteurii* via pore straining or wedging near grain-to-grain contact points, is critical for optimizing soil strength. To-date, there have been no reports on quantifying straining of *S. pasteurii* in saturated porous media.

The main purpose of this work is to explore the transport and fate of *S. pasteurii* in saturated sands under a wide range of ionic strengths (ISs from 0.5 to 1000 mM), flow velocities (50, 100, 200 cm/h), initial bacteria optical densities (1.0 and 0.48 OD₆₀₀), column lengths (280 and 150 mm), and under changes in IS conditions (i.e. 0.5 M CaCl₂ and DI water) in the context of bioaugmentation schemes for soil improvement via MICP. The straining profiles of bacteria under the tested IS conditions were obtained based on extruded sand segments after conducting breakthrough tests. We also tested the survival of *S. pasteurii* and its urease activity under a series of IS conditions (DI water, tap water, 500 and 1000 mM NaCl) to evaluate its adaptability under such low and high salinities. Finally, a two-site kinetic model, representing both attachment and straining of *S. pasteurii*, was calibrated and then applied to predict tracer and bacteria breakthrough curves using different IS conditions and bacteria concentration. This research can be used to provide model parameters for design of MICP-based bioaugmentation strategies for soil improvement.

2 Materials and Methods

2.1 Bacterial Culture

The ureolytically active bacterial strain *S. pasteurii* (DSMZ, DSM No. 33) were cultured in yeast extract media supplemented with urea (20 g/L) over a period of 24 h (at 30 °C and 115 rpm shaker). The cells were harvested by centrifugation of several 40-ml inoculated solutions in 50-ml tubes at a speed of 6000 g for 8 min. Then the centrifuged bacteria in each tube were re-suspended into 40-ml deionised (DI) water and centrifuged again to further remove any residual media that may cause continued bacterial growth. The desired optical density (1 OD₆₀₀ or 0.48 OD₆₀₀) of the bacteria was then achieved by diluting in either tap water or NaCl solution at various *IS* and was determined by a UV–VIS spectrophotometer at a wavelength of 600 nm. Figure 1a shows the OD₆₀₀ of *S. pasteurii* and the corresponding cell concentration ($C_{\text{cells/ml}}$) as measured at the University of Strathclyde (Steinacher 2021) on the same bacteria strain (DSM No. 33). $C_{\text{cells/ml}}$ at a given OD₆₀₀ is well-fitted by the empirical relationship by Ramachandran et al. (2001): $C_{\text{cells/ml}} = 8.59 \times 10^7 \times (\text{OD}_{600})^{1.3627}$. Zeta potential values of *S. pasteurii*, under varying *IS*, were measured (Fig. 1b) and used to evaluate the extended DLVO interaction energies.

2.2 Sand Characterization

Brown gravelly quartz sands (BAM Ritchies, UK) were selected for the column breakthrough tests. Particle-size distribution (SI Figure S1 in the Supporting Information) was determined by using US standard sieves according to ASTM D422. The median grain size (d_{50}) was determined as 490 μm. The uniformity index (d_{60}/d_{10}) was measured as 2.98. The sand samples were washed using DI water several times to remove impurities and fines that may affect the measurement of bacteria optical density. Prior to the column breakthrough tests, the oven-dried sand samples were autoclaved for 3 h to sterilise the sand. The zeta potential values of the sands, under varying *IS*, were measured and are plotted in Fig. 1b.

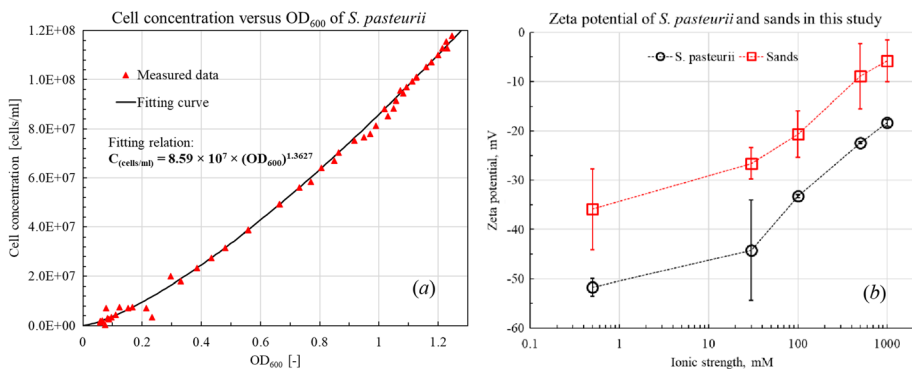


Fig. 1 **a** Empirical relation between cell concentration and bacteria OD₆₀₀ of *S. pasteurii*. The experimental data were cited from (Steinacher 2021) whilst the fitting relation was adopted from (Ramachandran et al. 2001). **b** zeta potentials of *S. pasteurii* and sands measured under ionic strengths of 0.5, 30, 500, 1000 mM NaCl

2.3 Column Breakthrough Experiments

Figure 2 shows the schematic diagram of the set-up used in the column breakthrough experiments. Sand was packed into polycarbonate columns with an inner diameter of 28 mm and an effective length of 280 mm. Screens were mounted at both inlet and outlet ends to evenly distribute 1-dimensional flow in the column. Prior to the bacterial breakthrough test, the sand columns were flushed with DI water for 10 min at a relatively high Darcy velocity (~ 400 cm/hour) to achieve a fully-saturated state and to further remove impurities and fines that may influence the measurement of bacteria density of effluent samples. A pore volume (PV) was defined as the change in mass (in grams) of the sand column before and after flushing with DI water (the small amount of water in the column head space was excluded). One PV of each 28-cm column was estimated to be ~ 50 cm³, assuming a density of water of 1 g/cm³. Note that this method may not precisely quantify the PV of each sand column, hence, a slight correction to PV was applied after fitting the tracer breakthrough curves (BTCs). The packing density of the sands in each column was calculated to be 1.75 ± 0.02 g/cm³, with a porosity of 0.29 ± 0.01 . The column breakthrough tests, under each condition as described below, were conducted in duplicate, triplicate or quadruplicate.

We set up the following four groups of experiments to study the effects of IS, flow velocity, initial bacteria density, and column size on the transport and fate of *S. pasteurii* in saturated sand columns. Details of the experimental conditions for the column breakthrough test are summarised in Table 1. Highlighted in bold are the controlled variables. For example, Experiment group 0 describes tracer breakthrough tests under three different flow velocities (50, 100, 200 cm/h), and Experiment group 1 describes bacteria breakthrough tests under an IS of 0.5, 30, 100, 500, 1000 mM.

Experiment 0 Tracer breakthrough test.

A tracer (NaCl) breakthrough test was conducted at the three flow (Darcy) velocities (50 cm/h, 100 cm/h, 200 cm/h) for the determination of the dispersion parameters. 3

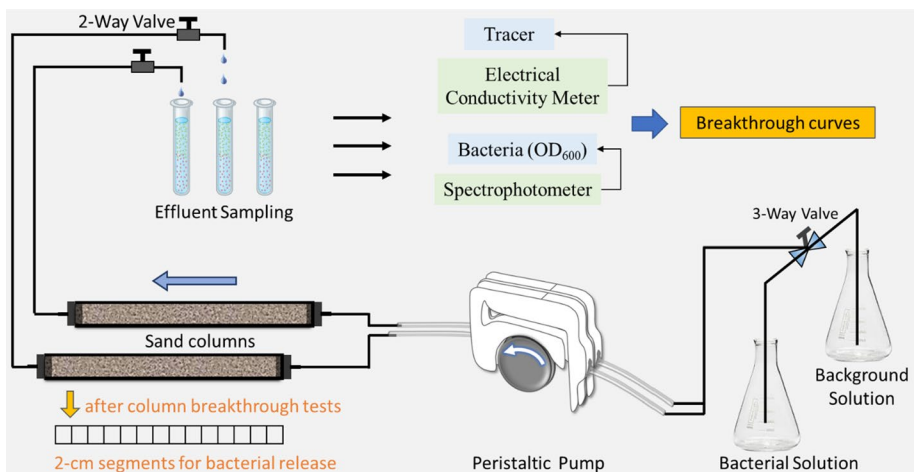


Fig. 2 Schematic diagram of column breakthrough experiment

Table 1 Experiments of the column breakthrough test

Experiment groups	Conditions for column experiments		Flow velocity u , cm/h	IS of Stage 1 solution, mM	IS of Stage 2 solution, mM
	Column length, mm	Initial OD ₆₀₀			
Experiment group 0 ^a Tracer only	280	N/A	50 100 200	100	DI water
Experiment group 1 ^b Effect of IS	280	1	100	0.5 (tap water) 30 100 500 1000	0.5 (tap water) 30 100 500 1000 1500 (0.5 M CaCl ₂)
Experiment group 2 ^c Effect of velocity & 0.5 M CaCl₂ in Stage 2	280	1	50 100 200	100	1500 (0.5 M CaCl ₂)
Experiment group 3 ^d Effect of initial OD₆₀₀ & 0.5 M CaCl₂ in Stage 2	280	0.48	100	100	1500 (0.5 M CaCl ₂)
Experiment group 4 ^e Effect of column length & DI Water elution	150	1	100	100 500	100 500

^aTracer breakthrough tests under flow velocities of 50, 100 and 200 cm/h;

^bBacteria breakthrough tests under ISs of 0.5, 30, 100, 500, 1000 mM NaCl;

^cBacteria breakthrough tests under velocities of 50, 100 and 200 cm/h (flushing 0.5 M CaCl₂ in Stage 2);

^dBacteria breakthrough tests under an initial OD₆₀₀ of 0.48 (flushing 0.5 M CaCl₂ in Stage 2);

^eBacteria breakthrough tests on short column under ISs of 100 and 500 mM NaCl (flushing 5 PVs DI water in Stage 3 (after Stage 2), which is not listed in the table)

PVs of 100 mM NaCl solution were injected at each velocity, followed by the injection of 3 PVs of DI water at the same velocity. The electrical conductivities of effluent samples were measured and the normalised breakthrough curves of tracer (NaCl) were obtained based on the linear relationship between electrical conductivity and ionic concentration.

Experiment 1 Effect of ionic strength (tap water, 30 mM, 100 mM, 500 mM, and 1000 mM NaCl).

In the first stage, 3 PVs of bacterial suspension with $OD_{600} = 1$ and prepared at each *IS* condition, i.e., tap water (electrical conductivity equivalent to that of 0.5 mM NaCl), 30 mM, 100 mM, 500 mM and 1 M NaCl solutions, were injected at a Darcy velocity of 100 cm/h. In the second stage, the 3-way valve was switched to continuously inject 3 PVs of bacteria-free background (NaCl or tap water) solution with the same *IS* and same flow velocity as applied in the first stage. The total 6 PVs of effluent samples were evenly distributed into 50 collection tubes with each one containing ~0.12 PV (~6 ml) solution. Electrical conductivity and OD_{600} of the effluent samples were determined using an electrical conductivity meter and a spectrophotometer at 600 nm, respectively. Normalised breakthrough curves of bacteria and tracer (NaCl) were obtained based on the linear relationship between electrical conductivity and ionic concentration, while normalised breakthrough curves of bacteria were obtained based on a relationship between OD_{600} and cell concentration for *S. pasteurii* (refer to Fig. 1a): $C_{cells/ml} = 8.59 \times 10^7 \times (OD_{600})^{1.3627}$. After the bacteria breakthrough experiment at each *IS* condition, the spatial distribution of the strained bacteria retained in each sand column was also obtained based on similar experimental protocols from previous studies (Bradford et al. 2002; Sang et al. 2013). Specifically, the sand samples were extracted from the column and segmented into fourteen 2-cm sections. Each section was gently immersed into 20 ml background NaCl (or tap water) solution with the same *IS* applied in the breakthrough experiment to release the bacteria retained exclusively by pore straining. Since there were no changes in ionic strength and negligible physical perturbation (gentle shaking), one can reasonably assume that there was a negligible release of the bacteria that were deposited on the grain surfaces due to attachment. These samples were left for 5 h to allow settlement of any fines that may interrupt the measurement of OD_{600} . Then the supernatant, i.e. the suspension containing the released bacteria was removed via a pipette and the OD_{600} was determined using a spectrophotometer.

Experiment 2 Effects of flow velocity (50 cm/h, 100 cm/h, 200 cm/h) and 0.5 M $CaCl_2$ solution.

At the first stage, 3 PVs of *S. pasteurii* ($OD_{600} = 1$) at an *IS* of 100 mM NaCl solution were injected under each flow (Darcy) velocity (50 cm/h, 100 cm/h, 200 cm/h). At the second stage, instead of injecting 3 PVs of background NaCl solution, 3 PVs of 0.5 M bacteria-free $CaCl_2$ solution (with a much stronger *IS* than that of a 100 mM NaCl solution) were injected under the same flow velocity to reproduce the injection of cementing solution during MICP treatment. This process caused an enhancement of the *IS* (from 100 to 1500 mM); The three velocities (50 cm/h, 100 cm/h, 200 cm/h) were selected to approximately cover the velocity range of radial flow (influential area: diameter = 1 m) around an injection well, based on an injection rate of ~20 L/minute and an injection depth of 1 m.

Experiment 3 effect of bacteria density (0.48 OD₆₀₀).

Similar to Experiment 2, 3 PVs of *S. pasteurii* (OD₆₀₀=0.48) at an *IS* of 100 mM NaCl solution and a flow velocity of 100 cm/h were flushed in the first stage, followed by an injection of 3 PVs of 0.5 M CaCl₂ solution at a flow rate of 100 cm/h in the second stage. The final bacterial breakthrough curve was normalised by the initial bacterial concentration at an OD₆₀₀ of 0.48.

Experiment 4 Effects of column size and DI water elution.

To study the effect of column size on bacterial transport, breakthrough experiments were conducted in 52-mm diameter and 150-mm length columns at a flow velocity of 100 cm/h. At the first stage, 3 PVs of *S. pasteurii* (OD₆₀₀=1) at *IS*s of 100 mM or 500 mM (NaCl) were injected, followed by an injection of 3PVs of background NaCl solution at the second stage with the same *IS* and same flow velocity as applied in the first stage. At last, 5 PVs of DI water were flushed at the same velocity.

2.4 Bacterial Survival Under High *IS*

Bioaugmentation typically involves a two-phase grouting strategy i.e. Phase 1—augmenting/injecting bacteria solution, and Phase 2—Circulation of cementing solution CaCl₂ & Urea. Between the two phases there may, or may not, exist a short static (no-flow) period for bacterial settlement. To explore the survival of *S. pasteurii* and its effectiveness for urea hydrolysis especially under high *IS* conditions (i.e. 500 and 1000 mM) within the timescales required for bioaugmentation, we conducted 5 sets of urease activity tests and OD₆₀₀ tests (each set in duplicate). Specifically, after 24-h culturing in the yeast extract media the *S. pasteurii* were centrifuged and re-suspended either into DI water, tap water, 500 mM NaCl solution, 1000 mM NaCl solution or the originally centrifuged media. After 5-h static period, 2 ml re-suspended bacteria (OD₆₀₀=0.75) in the above solutions were re-inoculated into 40 ml fresh media. After 24-h incubation at 30 °C and on a 115-rpm shaker, bacteria OD₆₀₀ and specific urease activity, which quantifies the rate of urea hydrolysis (unit: mM/min/OD₆₀₀) for MICP, were measured and compared to evaluate the influence of high NaCl concentration (500 and 1000 mM) on the effectiveness of *S. pasteurii*. The experimental results indicated that the effect of high salinity (up to 1000 mM) on bacteria survival and activity was negligible (refer to SI Figure S2 in the supporting information for more details).

2.5 Two-site Kinetic Modelling

The transport of bacteria and tracer in homogeneous and saturated porous sand columns can be described by the following two equations (Tan et al. 1994), respectively.

$$\frac{\partial(\phi C)}{\partial t} + \frac{\partial(\rho_b S)}{\partial t} = \nabla \cdot \phi \mathbf{D} \nabla C - \mathbf{u} \cdot \nabla C - R_d + R_g \quad (1)$$

$$\frac{\partial(\phi c)}{\partial t} = \nabla \cdot \phi \mathbf{D} \nabla c - \mathbf{u} \cdot \nabla c \tag{2}$$

where ϕ [-] is water-filled porosity of the sand column; C [N_c/L^3] is the bacterial concentration suspended in the solution (number of cells per unit volume of the aqueous solution) and c [M/L^3] is the concentration of the tracer; t is time [T]; S [N_c/M] is the bacterial concentration deposited on the solid particles (number of cells per unit mass of solid particles); ρ_b [M/L^3] is the bulk density of the dry sand column; Accordingly, $(\rho_b \cdot S/\phi)$ is the deposited bacterial concentration defined as the number of bacterial cells attached on the solid particles per unit volume of pore-solution. \mathbf{u} [L/T] is the Darcy velocity; R_d and R_g are the rates [$N_c/L^3/T$] of bacterial decay and growth, respectively; \mathbf{D} [L^2/T] is the dispersion coefficient of the bacteria, which is a function of the hydrodynamic dispersivity α [L] and effective diffusion coefficient d_c [L^2/T] (Minto et al. 2019; Tobler et al. 2014).

$$\mathbf{D} = \alpha \mathbf{u} / \phi + d_c \tag{3}$$

Assuming that there is negligible bacterial decay and growth during the transport process, the bacterial concentration (S) deposited on the solid particles can be governed by a two-site kinetic model (Bradford et al. 2013; Foppen et al. 2007), which defines attachment (S_1) on the surfaces of soil particles (site 1) and pore straining (S_2) at crevices and constrictions (site 2). The total number of deposited bacteria equals the sum of bacterial retention in both sites as $S = S_1 + S_2$. The two-site deposition model is given by the following two equations.

$$\frac{\rho_b}{\phi} \frac{\partial S_1}{\partial t} = K_{attach0} \psi_1 C - \frac{\rho_b}{\phi} K_{detach0} S_1 \tag{4}$$

$$\frac{\rho_b}{\phi} \frac{\partial S_2}{\partial t} = K_{strain0} \psi_2 C \tag{5}$$

where $K_{attach0}$ [1/T] is the initial first-order attachment rate; $K_{detach0}$ [1/T] is the detachment rate due to hydrodynamic shear; $K_{strain0}$ [1/T] is the initial first-order straining rate. Here, we assume that pore straining (S_2) is an irreversible process and there is no term for bacteria release in Eq. (5). ψ_1 and ψ_2 in Eqs. (4) and (5) are dimensionless decay functions for site 1 (attach) and site 2 (straining) respectively. Decay of the attachment rate could be attributed to a decreasing number of collisions between suspended bacteria and grains according to colloid filtration theory. Whereas, decay of the straining rate is due to blocking or filling at the crevices and constrictions as straining proceeds. To model the decay of the attachment rate and straining rate due to a decrease in collisions between bacteria and grains or site blocking, both ψ_1 and ψ_2 decrease with increasing bacterial retention in each site (Gargiulo et al. 2008; Liao et al. 2021; Sasidharan et al. 2014). In this study, we adopt an exponential form (Xu et al. 2006; Xu and Saiers 2009) of the decaying functions, given by

$$\psi_1 = e^{-S_1/\lambda_1} \tag{6}$$

$$\psi_2 = e^{-S_2/\lambda_2} \tag{7}$$

where $1/\lambda_1$ and $1/\lambda_2$ are the decay constants of bacterial attachment (site 1) and straining (site 2), respectively. λ_1 and λ_2 have the same dimension as S [N_c/M] and quantifies the exponential decline in rates of attachment and pore straining.

The total mass recovery of the bacteria is defined as the total accumulation of effluent bacteria passing through the outlet divided by the total accumulation of bacteria injected at the inlet.

$$M_r = \frac{\int_0^{t_{end}} C(L, t)uAdt}{\int_0^{t_0} C(0, t)uAdt} = \frac{\int_0^{t_{end}} C(L, t)dt}{\int_0^{t_0} C(0, t)dt} \tag{8}$$

where L [L] and A [L^2] are the length and cross-sectional area of the column respectively. $C(0, t)$ and $C(L, t)$ are bacterial concentrations at the inlet and outlet at time t , respectively. t_0 [T] is the duration of bacterial injection, t_{end} is the total duration from the beginning of bacterial injection to the end of the target stage.

The above transport model was solved by the finite-element-based COMSOL Multiphysics to fit and validate the 1-dimensional column test results. The geometry contained 280 domain elements with the mesh size being 1 mm. The initial condition, inlet and outlet boundary conditions are given by,

$$\text{Initial condition : } C(t = 0, x) = \begin{cases} 0 & \text{in Stage1} \\ \text{value of last step in Stage1} & \text{in Stage2} \end{cases} \tag{9}$$

$$\text{Inlet boundary : } C(t, x = 0) = C_{inlet} \tag{10}$$

$$\text{Outlet boundary : } \frac{\partial}{\partial x} C(t, x = L) = 0 \tag{11}$$

where x is the distance to inlet. The initial concentration of tracer and bacteria was set to 0 during the 1st Stage (i.e., the injection of bacteria solution). Then, the value of final step in the 1st Stage was used as the initial condition for the 2nd stage (i.e., flushing). The inlet boundary for bacteria transport was: $C_{inlet} = 1 \text{ OD}_{600}$ (or 0.48 OD_{600} in Experiment 3) during flushing with a bacteria solution ($C_{cells/ml} = 8.59 \times 10^7 \times (\text{OD}_{600})^{1.3627}$); $C_{inlet} = 0 \text{ OD}_{600}$ during flushing with a bacteria-free solution. The inlet boundary for tracer transport was given by the realistic ionic strengths, i.e. $c_{inlet} = 0.5, 30, 100, 500,$ or 1000 mM for Experiment 1, $c_{inlet} = 1500 \text{ mM}$ for flushing 0.5 M CaCl_2 in Experiments 2&3 during the 2nd stage, and $c_{inlet} = 0 \text{ mM}$ for flushing DI water in Experiment 4 during the 3rd stage.

The attachment/straining rates under the injection of 0.5 M CaCl_2 solution are defined as follows.

$$k_{attach} = \left(K_{attach0} + \frac{I_S - I_{S1}}{I_{S2} - I_{S1}} \Delta K_{attach} \right) e^{-S_1 / \left(\lambda_1 + \frac{I_S - I_{S1}}{I_{S2} - I_{S1}} \Delta \lambda_1 \right)} \quad I_{S1} \leq I_S \leq I_{S2} \tag{12}$$

$$k_{strain} = \left(K_{strain0} + \frac{I_S - I_{S1}}{I_{S2} - I_{S1}} \Delta K_{strain} \right) e^{-S_2 / \left(\lambda_2 + \frac{I_S - I_{S1}}{I_{S2} - I_{S1}} \Delta \lambda_2 \right)} \quad I_{S1} \leq I_S \leq I_{S2} \tag{13}$$

where I_{S1} and I_{S2} are the realistic ionic strengths of the 100 mM NaCl solution ($I_{S1} = 100 \text{ mM}$) and 0.5 M CaCl_2 solution ($I_{S2} = 1500 \text{ mM}$), respectively. ΔK_{attach} and ΔK_{strain} are the enhanced attachment rate and straining rate, respectively. $\Delta \lambda_1$ and $\Delta \lambda_2$ are the changes in decay constants under the injection of 0.5 M CaCl_2 . Equations (12) and (13)

indicate that the retention parameters will be enhanced once the moving front of the CaCl_2 solution ingresses (i.e. $I_S > I_{S1} = 100\text{mM}$), until it reaches a steady equilibrium value (i.e. $I_S = I_{S2} = 1500\text{mM}$).

Similarly, for Experiment 4 during the 3rd Stage, the injection of 5 PVs of DI water also caused a gradual decrease in IS. Hence, the release of bacteria due to DI water elution is modelled by introducing an increase in the detachment rate k_{detach} as follows.

$$k_{detach} = K_{detach0} + \Delta K_{detach} \left(1 - \frac{I_S}{I_{S1}} \right) \quad 0 \leq I_S \leq I_{S1} \tag{14}$$

where ΔK_{detach} is the increment of the detachment rate under the elution of DI water.

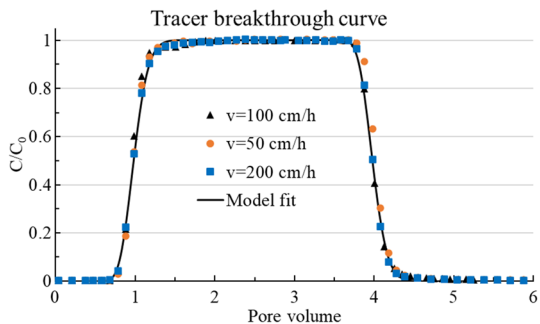
3 Results and Discussion

3.1 Transport of a Conservative Tracer

Figure 3 shows the observed and modelled BTCs of the tracer NaCl (normalised) during injection of 3 PVs of 100 mM NaCl followed by injection of 3PVs of DI water. The hydrodynamic dispersivity (α) and the effective diffusion coefficient (d_c) were determined as 3×10^{-3} m and 1×10^{-9} m²/s, respectively, which were independent of flow velocity. The fitted result indicates that that diffusion is negligible compared to hydrodynamic dispersion within the range of velocities tested.

Normalised BTCs of the conservative tracer for Experiments 1–4 were also determined (refer to SI Figure S3-S5). Based on the same hydrodynamic dispersivity (3×10^{-3} m) and effective diffusion coefficient (1×10^{-9} m²/s) as used for Experiment 0, the modelled tracer BTCs for Experiments 1–4 show a good match with the experimental results (SI Figure S3-S5). This validates that NaCl can serve as a non-reactive tracer, consistent with a previous study by Vasiliadou and Chrysikopoulos (2011). The good agreement between the experimental and modelled results also reflects well-packed sand columns with no notable signs of preferential flow paths or “wall effects”. For all Experiments 0–4, the tracer (NaCl) started to breakthrough at ~0.6 PV of the bacteria solution and reached equilibrium at ~1.6 PV. This indicates that the dispersion effect is non-negligible. Otherwise, both the breakthrough and the equilibrium would occur at 1PV.

Fig. 3 Experimental and modelled breakthrough curves of the tracer (NaCl) in saturated sand columns at different velocities (50 cm/h, 100 cm/h, 200 cm/h) for Experimental 0



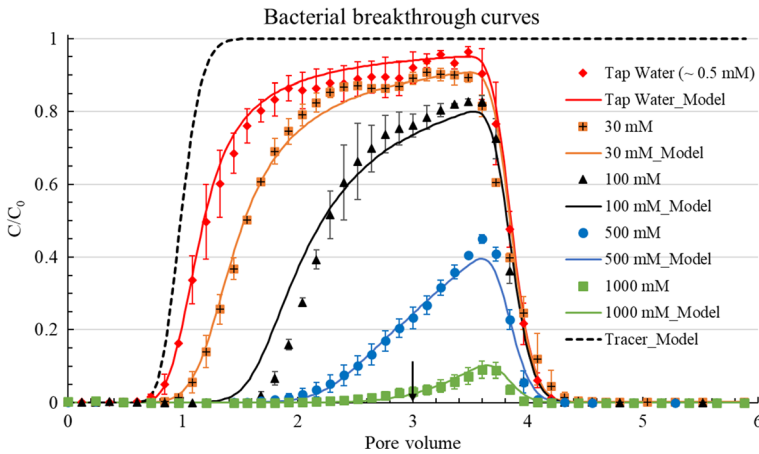


Fig. 4 Experimental and modelled bacterial BTCs (normalised) under different *IS* conditions (Experiment 1). Error bars represent standard deviations in results from replicate experiments. The modelled tracer BTC is also plotted (black dash line) for comparison. Black arrow marks where the injection of bacterial solution was changed to the background solution

3.2 Transport and Retention of Bacteria

3.2.1 Experiment 1: Effect of Ionic Strength

Figure 4 shows the observed and modelled bacterial BTCs (normalised) under different *IS* conditions (Experiment 1). Compared to the conservative tracer, as shown by the black dashed line in Fig. 4 (the experimental tracer BTCs are shown in SI Figure S3), breakthrough of the bacteria is more delayed and reaches a lower concentration, due to bacterial retention. This behavior becomes more obvious as the *IS* increases from 0.5 to 1000 mM. It is also evident in Fig. 4 that after injection of 3 PVs of bacterial solution, i.e. during injection of 3 PVs of the bacteria-free background solution, the bacteria concentration in the BTCs continues to increase for another ~0.6 PV, before sharply declining. The continuous increase of the BTCs is attributed to the displacement of bacteria in the pore solution (injected during Stage 1), whilst the sharp decline in bacterial breakthrough without notable “tailing” indicates negligible detachment.

The two-site kinetic model was calibrated using the bacterial BTCs (Fig. 4) and the straining profiles (Fig. 5) under *IS*s of 0.5–1000 mM. The increase of ionic strength from 0.5 to 1000 mM enhanced the attachment of *S. pasteurii* from 9.4 to 69.6% (model: 6.7% to 67.8%) as shown in Table 2. Figure 6 shows the interaction energies between *S. pasteurii* and quartz sands, and between *S. pasteurii* cells, as a function of separation distance, which were calculated based on the measured zeta potential values (Fig. 1b) according to the extended DLVO theory (Hahn et al. 2004; Hogg et al. 1966). As *IS* increased from 0.5 to 1000 mM, the interaction energy shifts from an energy barrier (unfavourable conditions for retention at 0.5 mM) to the appearance of secondary energy minima (30 and 100 mM) and primary energy minima (500 and 1000 mM), thus leading to an increase in the attachment on grain surfaces. This is consistent with a recent study by Jain and Arnepalli (2020) who also demonstrated an enhanced attachment of *S. pasteurii* (strain type: ATCC 11859) with increasing *IS* from 0.1 to 100 mM in saturated sand columns. Note that the bacteria

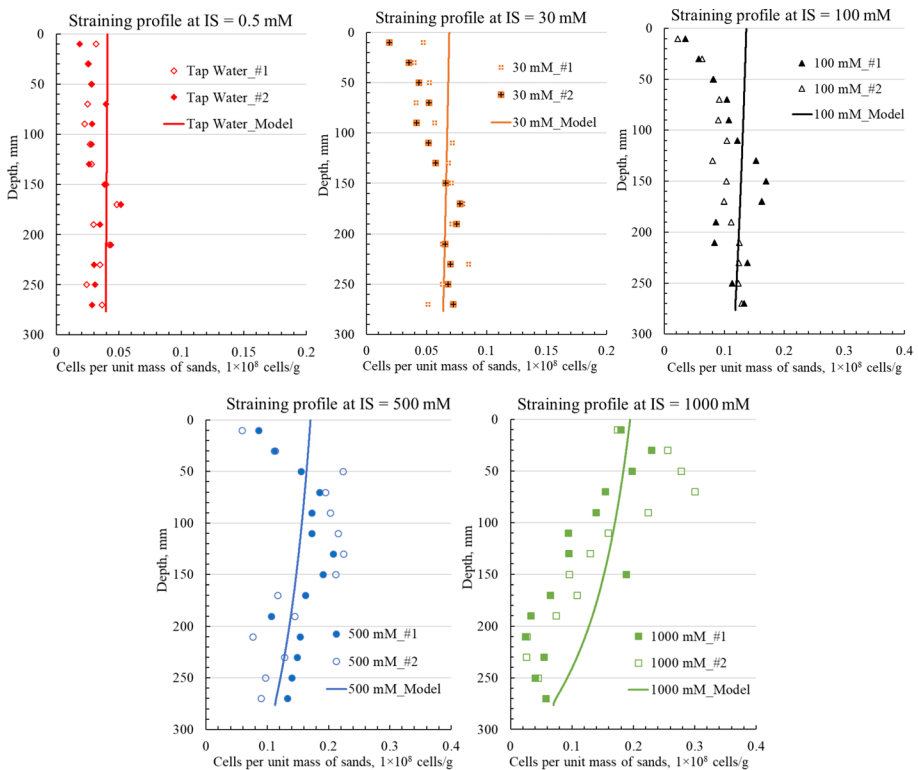


Fig. 5 Experimental and modelled deposition profiles due to pore straining along the column length under different ionic strength conditions (Experiment 1)

breakthrough curves at 30 and 100 mM in this study show higher breakthrough bacteria concentrations than those by Jain and Arneppalli (2020). This occurs because the bacteria strains (DSM No. 33) and sands in our study had smaller zeta potential values (more negative) at the same IS conditions (i.e. 30 and 100 mM). This demonstrates that even for the same bacteria, calibration of model parameters is required, since there can be significant variation between different type strains.

As IS increased from 0.5 to 1000 mM (Fig. 5), straining of *S. pasteurii* was increased from 8.1 to 28.2% (model: 8.0 to 29.8%). Straining is well-known to be influenced by pore space geometry (McDowell-Boyer et al. 1986), solution chemistry and hydrodynamics (Bradford et al. 2006, 2007; Foppen et al. 2007; Torkzaban et al. 2008b). (Bradford et al. 2002, 2007) reported that straining occurs in colloid deposition when the ratio of colloid diameter to median grain size (d_p/d_g) is as low as 0.2%. The *S. pasteurii* cells (DSM No. 33) in this study are rod shaped, with a length of $\sim 2\text{--}8\ \mu\text{m}$ and a diameter of $\sim 0.5\text{--}0.8\ \mu\text{m}$ (microscopic image in SI Figures S6 & S7), giving d_p/d_g values approximately 0.1% to 1.0% based on the average rod diameter and average length, respectively. Under chemically unfavorable condition (IS=0.5 mM), straining only accounted for 8.1% of the total injected bacteria solution. With the increase of IS to 100 mM, bacterial straining increased to 22.9% (model: 25.8%), possibly due to the increased number of bacteria in the secondary energy minimum which are prone to funneling and retention in the small pores formed

Table 2 Fitting parameters of the two-site kinetic model and mass recovery. Dispersivity $\alpha = 3 \times 10^{-3}$ m; effective diffusion coefficient $d_e = 1 \times 10^{-9}$ m²/s

Scenarios	Experimental condition	Site 1 (attach/detach)		Site 2 (straining)		Total recovery		Total attachment		Total straining		
		$K_{attach0}$ 1/s	λ_1 $\times 10^8$ cells/g	$K_{detach0}$ 1/s	$K_{strain0}$ 1/s	λ_2 $\times 10^8$ cells/g	Exp	Model	Exp	Model	Exp	Model
Experiment 1 ^a (calibration)	$IS = 0.5$ mM	2.0×10^{-3}	0.01	0	4.0×10^{-3}	0.01	82.5	85.3	9.4	6.7	8.1	8.0
	$IS = 30$ mM	8.0×10^{-3}	0.02	0	1.0×10^{-2}	0.015	70.6	70.9	17.0	15.8	12.4	13.3
	$IS = 100$ mM	1.0×10^{-2}	0.04	0	4.0×10^{-2}	0.025	45.3	47.7	31.8	26.5	22.9	25.8
	$IS = 500$ mM	1.2×10^{-2}	0.15	0	6.0×10^{-2}	0.03	14.9	14.4	50.9	56.1	34.2	29.5
	$IS = 1000$ mM	1.6×10^{-2}	0.25	0	6.2×10^{-2}	0.035	2.3	2.4	69.6	67.8	28.2	29.8
Experiment 2 ^b (calibration)	$u = 50$ cm/h	2.0×10^{-2}	0.04	0	4.0×10^{-2}	0.04	18.3	20.0	N/A	39.5	N/A	40.5
	$u = 100$ cm/h	1.0×10^{-2}				0.025	40.7	44.7	29.5	29.5	25.8	25.8
Experiment 3 ^c (validation)	$u = 200$ cm/h	8.0×10^{-3}				0.02	46.9	58.3	22.4	22.4	19.3	19.3
	$OD_{600} = 0.48$	1.0×10^{-2}	0.04	0	4.0×10^{-2}	0.025	15.8	16.9	40.9	40.9	42.2	42.2
Experiment 4 ^d (validation)	$L = 150$ mm	1.0×10^{-2}	0.04	0	4.0×10^{-2}	0.025	56.6	56.5	21.5	21.5	22.0	22.0
	$IS = 100$ mM											
	$L = 150$ mm		0.15	0	6.0×10^{-2}	0.03	25.4	29.0	45.0	45.0	26.0	26.0
	$IS = 500$ mM											

^aModel parameters were calibrated based on bacteria breakthrough curves and straining profiles in Fig. 4 and Fig. 5;

^bNote, model parameters at a flow velocity of 100 cm/h (& 100 mM IS) are the same as those in Experiment 1 at IS = 100 mM (& 100 cm/h)

^cModel parameters taken from Experiment 1 with IS = 100 mM

^dModel parameters taken from Experiment 1 with IS = 100 mM or 500 mM, as appropriate

In addition, for Experiments 2 and 3 during the 2nd stage (i.e. the injection of 3 PVs of 0.5 M CaCl₂ solution), the attachment and straining rates (refer to Eqs. (12) and (13)) were enhanced by 8.6×10^{-3} [1/s] (ΔK_{attach}) and 4×10^{-2} [1/s] (ΔK_{strain}), respectively, with their decay constants $\Delta\lambda_1$ and $\Delta\lambda_2$ enhanced by 0.34×10^8 and 0.01×10^8 cells/g, respectively. For Experiment 4 during the 3rd stage, the injection of 5 PVs of DI water caused bacterial release. The increment of the detachment rate ΔK_{detach} (refer to Eq. (14)) was 4×10^{-3} and 8×10^{-4} [1/s] respectively for the two cases

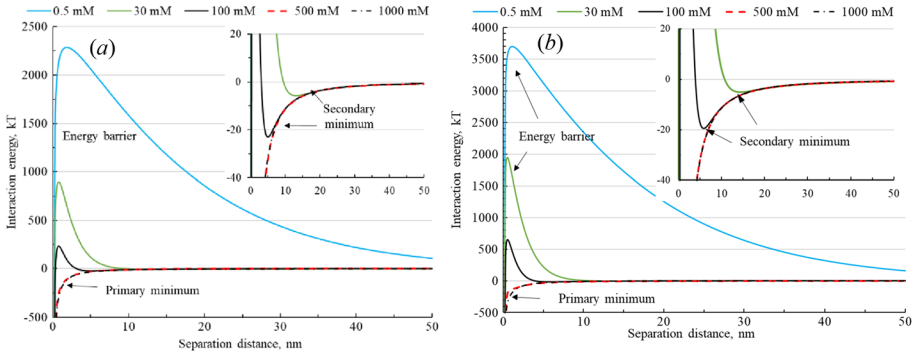


Fig. 6 **a** DLVO interaction energy between *S. pasteurii* and quartz sands and **b** between bacterial cells as a function of separation distance under different ISs. The insets mark the secondary energy minimum

adjacent to grain–grain junctions (Bradford et al. 2007; Torkzaban et al. 2008a). With further IS increases to 500 and 1000 mM, straining increased to 34.2% and 28.2% respectively. Microscopic images of *S. pasteurii* cells under ISs of 0, 100, 500 and 1000 mM (refer to SI Figures S6 & S7) show that coagulation of 2–3 bacterial cells occurs under ISs of 500 and 1000 mM whilst almost no bacterial coagulation is observed under ISs of 0 and 100 mM. Hence, the increased straining at from 100-mM IS to 500- and 1000-mM IS could be a result of bacterial coagulation.

Figure 5 also shows an overall decrease in bacterial straining with increasing depth, and the decreasing trend is more obvious at higher IS (especially at 1000 mM). Bradford et al., (2003, 2005, 2006) applied a time- and depth- dependent straining function to describe this phenomenon. In this study, we use an exponential decay of strain rate due to site-blockage effects, as adopted from Xu et al. (2006) and Xu and Saiers (2009), to model

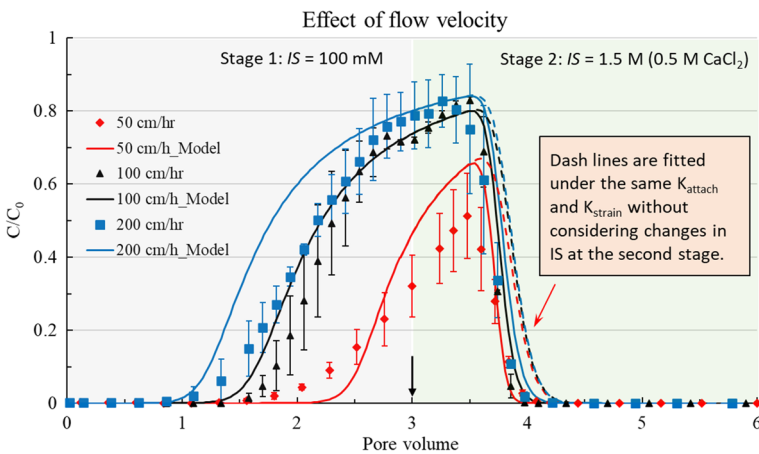


Fig. 7 Experimental and modelled bacterial breakthrough curves under different flow velocity conditions (Experiment 2). Error bars represent standard deviations in results from replicate experiments. Due to the enhancement of the IS at Stage 2, the overall attaching/straining rates were enhanced accordingly. Black arrow marks where the injection of bacterial solution was changed to 0.5 M CaCl₂ solution

the observation of decreasing straining with increased distance from the inlet (Fig. 5). Note that the straining profiles at depths of 0–50 mm (Fig. 5) deviate from this decreasing trend with increasing depth, possibly due to increased fluid velocities near the inlet where radial flow is approached at the point of injection, which results in increased hydrodynamic shear forces and hence the potential to release strained bacteria if the fluid velocity exceeds a critical value (Bradford et al. 2006). This hydrodynamic shearing of strained bacteria might also account for the higher percentage of straining observed at 500 mM IS (34.2%) than at 1000 mM (28.2%). The release of bacteria cells from straining was not captured in our model which assumed pore straining is an irreversible process.

3.2.2 Experiment 2: Effects of Flow Velocity and 0.5 M CaCl₂ Solution

Figure 7 shows the observed and modelled bacterial BTCs (normalised) under different velocity conditions and with injection of 0.5 M CaCl₂ in Stage 2 (Experiment 2). The total recovery of bacteria under velocities of 50, 100, and 200 cm/h was 18.3%, 40.7%, and 46.9% respectively, according to the experimental BTCs. The increasing bacterial recovery, or decreasing bacterial retention, with increasing flow velocity (from 50 to 200 cm/h) can be attributed to both a decrease in attachment (from 35.9 to 22.4%) and a decrease in straining (from 40.5 to 19.3%). Firstly, higher flow velocities create greater hydrodynamic shear forces, which act to offset the attractive forces between the bacteria and the grains and hence reduce the rate of attachment at secondary energy minima (Fig. 6a; IS = 100 mM). Note that Experiment 1 in Sect. 3.2.1 observes no obvious “tailing” at the same IS (100 mM) and at a velocity of 100 cm/h (Fig. 4). This indicates that the rate of detachment is negligible at IS = 100 mM with a velocity no greater than 100 cm/h (e.g. 50 and 100 cm/h). At a flow velocity of 200 cm/h and at IS = 100 mM, the detachment rate may not be negligible, and is a topic for future studies. Secondly, the increased hydrodynamic forces as a result of the increasing flow velocity also tends to (1) decrease the extent of flow stagnation regions; and (2) decrease the weakly-attached bacteria at the secondary energy minimum which can then be funneled into small regions of pore space formed adjacent to grain–grain junctions (Bradford et al. 2007). Both effects could potentially decrease bacterial straining (Bradford et al. 2007; Torkzaban et al. 2008a, 2008b). In this study, the decreasing straining with increasing flow velocity (50–200 cm/h) was modelled by an increase in the decay constant $1/\lambda_2$ at the straining site (i.e. λ_2 decreased from 0.04 to 0.02×10^8 cells/g).

Unlike in Experiment 1, which created no changes in ionic strength due to the injection of 3 PVs of background solution (at the same IS) in Stage 2, in Experiment 2 we injected 3 PVs of 0.5 M CaCl₂ solution in Stage 2 to reproduce the commonly applied cementation fluids in MICP treatment strategies. This caused a discrepancy between the observed and modelled BTCs if changes to the retention parameters were not modelled (dashed lines in Fig. 7). By simulating the effect of the increased IS in the injection fluid on the disturbed retention parameters, as shown in the annotation in Table 2 and according to Eqs. (12) and (13), the two-site kinetic model was able to accurately reproduce the experimental BTCs during Stage 2 (solid lines in Fig. 7). Comparing the bacterial BTCs of Experiment 1 (Fig. 4) with Experiment 2 (Fig. 7), the injection of the stronger IS (0.5 M CaCl₂) solution tends to stabilise the pre-attached and pre-strained bacteria rather than remove or mobilise them, as indicated by the more steeply declining slope of the post-peak BTCs between 3.6 and 4 PVs.

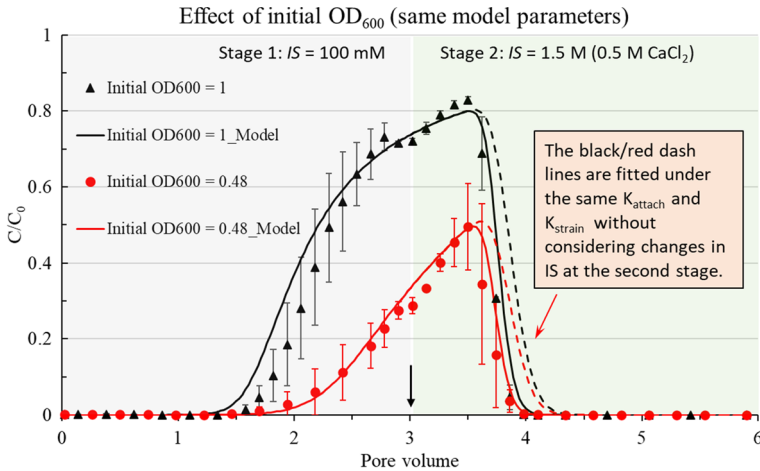


Fig. 8 Experimental and modelled bacterial breakthrough curves under initial OD_{600} of 1 and 0.48 (Experiment 3). Error bars represent standard deviations in results from replicate experiments. Black arrow marks where the injection of bacterial solution was changed to 0.5 M $CaCl_2$ solution

3.2.3 Experiment 3: Effect of Initial Bacteria Density

Figure 8 shows the observed normalised bacterial BTCs (marked by black triangles and red dots) under the initial OD_{600} of 1 and 0.48 (flow velocity: 100 cm/h; Stage 1: 100 mM bacterial solution; Stage 2: 0.5 M $CaCl_2$ solution). Based on the model parameters calibrated in Experiment 1 for an $OD_{600} = 1$, the modelled bacterial BTC (normalised) under the initial OD_{600} of 0.48, as marked by the red solid line in Fig. 8, also shows a good match with the experimental observation. This verifies that the model is capable of describing the bacteria transport and retention process, regardless of the initial bacteria concentration. As seen in Table 2, the total bacteria masses recovered at the outlet for OD_{600} values of 1 and 0.48, were 45.3% (model: 47.7%) and 15.8% (model: 16.9%), respectively, with the attachment enhanced from 31.8 (model: 26.5%) to 40.9% (model only), and straining enhanced from 22.9% (model: 25.8%) to 42.2% (model only). The lower mass recovery or higher bacterial retention at 0.48 OD_{600} is attributed to a lower site-blocking effect, which enhances the overall attachment and straining rates throughout the sand column. Specifically, according to Eqs. (4) & (5), the numbers of cells deposited at grain surfaces (attachment S_1) and pore throats or grain contact points (straining S_2) increases more slowly for a lower initial bacteria concentration (C_0), which in turn causes a smaller decay (ψ_1 and ψ_2) of the attachment/straining rate – as indicated by Eqs. (6) & (7). Therefore, the injection of a lower initial bacteria concentration causes less site-blocking and hence results in more efficient bacterial retention.

3.2.4 Experiment 4: Effect of Residence Time and DI Water Elution

The observed bacterial BTCs in short columns (length: 150 mm) under IS s of 100 mM and 500 mM for Stage 2 of Experiment 4 are shown in Fig. 9a and b respectively, plotted against the previous results for the longer column (length: 280 mm) in Experiment 1. Compared to the bacterial BTC for longer column experiments, shorter columns exhibited

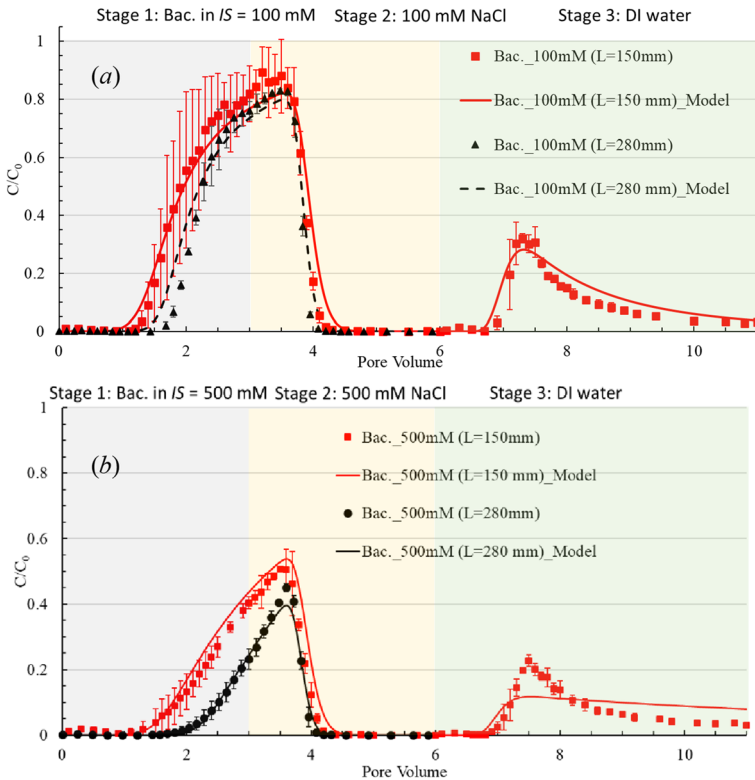


Fig. 9 Experimental and modelled bacterial (and tracer) breakthrough curves in shorter columns (length: 150 mm) under two IS conditions: **a** 100 mM; **b** 500 mM (Experiment 4). Error bars represent standard deviations in results from replicate experiments. Flushing of 5 PVs of DI water leads to a partial bacterial detachment in stage 3

a higher bacterial breakthrough at the same “PV” value (i.e. x -coordinate; note that the PV is not an absolute value but a relative value based on each column). This occurs because, since the column length is almost halved and the fluid velocity remains the same, the time taken for fluid to pass from the inlet to the outlet of the shorter column is also almost halved. At the same PV, the shorter residence time for fluid in the short column implies that less time is available for attachment/straining and, hence, the bacteria breakthrough is higher. (Tobler et al. 2014) also showed a decrease in bacterial (*S. pasteurii*) mass recovery with increasing column length. Figure 9a and b shows the modelled bacterial BTCs based on the previously calibrated parameters from Experiment 1. The model results show a good fit to the experimental data, which again demonstrates that the proposed two-site kinetic model can describe the transport process, regardless of column geometry.

The flushing of 5 PVs DI water at Stage 3 was conducted on the 52-mm diameter columns only, and caused a bacterial release, as shown in Fig. 9a and b. (Hahn et al. 2004; Sang et al. 2013) attributed the release of particles/colloid under the elution of DI water to the reversible deposition at shallow secondary minima while deposition at deep primary minima is irreversible. (Choi et al. 2017), however, points out that part of the bacteria attached by primary minimum can be detached under the elution of lower IS solution and

thus contribute to the reversible attachment. The appearance of the secondary minimum and energy repulsion under DI water elution leads to a partial bacterial detachment at shallow minimum (or at energy barrier). From Fig. 9a and b, the two-site kinetic model, provides a good match to bacterial release under the application of DI water during Stage 3. Modelling predictions estimate the total mass recovery at the end of Stage 3 under *IS*s of 100 mM and 500 mM were 74.4% and 42.4%, respectively, with the mass recovery during Stage 3 alone being 17.9% and 13.4% respectively.

4 Implications for Field Applications of MICP

Microbially induced calcite precipitation via ureolysis has been widely applied in energy research including removal of radionuclide contaminants in groundwater (Fujita et al. 2008), soil stabilization (DeJong et al. 2010; Whiffin et al. 2007), remediation of subsurface rocks (Cuthbert et al. 2013; Minto et al. 2016), wellbore sealing (Phillips et al. 2016) and CO₂ capture and storage (Mitchell et al. 2010; Phillips et al. 2013) among others. Almost all of these bioremediation applications involve a transport and retention process to achieve an effective delivery of the ureolytic microbes into porous or fractured media. Our study shows that the transport and fate of ureolytic *S. pasteurii* in saturated sand columns is highly dependent on the aqueous chemistry, flow velocity, bacteria density, as well as the bacteria residence time in the soil. This causes the extreme complexity of bacterial transport and retention under real field conditions at temporal and spatial scales. However, the complexity and challenges associated with MICP treatment could be overcome if bacterial retention mechanisms are well understood and, hence, can be accurately modelled. Our study provides a method for quantification and prediction of bacterial transport and fate in 1-dimensional saturated sand columns, which may be upscaled to a 3-dimensional real field with different *IS* conditions and with a non-uniform velocity distribution. This modelling approach can then be incorporated into 3D reactive transport models of the MICP process (Minto et al. 2019). El Mountassir et al., (2018) outlined some of the challenges associated with MICP treatment. Based on the observations and results presented herein some strategies to overcome these challenges are presented.

Challenge 1 Clogging near injection well and uniformity

Many laboratory-scale experiments have shown increased carbonate precipitation near the inlet (Tobler et al. 2012; Whiffin et al. 2007). The results presented here demonstrate that the retention of *S. pasteurii* can be reduced by increasing the flow velocity. Hence, clogging at the injection point could be reduced by increasing the flow rate at the injection point (since under radial flow conditions velocity decreases exponentially with radial distance from the injection point so this will only remobilise bacteria close to the well), or by applying a small pulse of low *IS* water to mobilise *S. pasteurii* in the volume immediately surrounding the injection well.

In particular for applications where strength gain is the target outcome, uniformity of carbonate precipitation is desirable (Barkouki et al. 2011). A relatively homogeneous bacterial retention in porous media may be achieved by pumping of bacterial and cementing solutions under appropriate aqueous chemistries (Yang et al. 2022), thus promoting effective MICP soil stabilization. For example, our study demonstrates that the injection of 0.5 M CaCl₂, as is commonly conducted in MICP injection strategies (i.e. as part of cementing solution), has been shown to stabilise pre-attached and pre-strained *S. pasteurii*, limiting cell re-entrainment; On the contrary, the injection of DI water with a much lower

ionic strength leads to a partial detachment of *S. pasteurii*. Thus, between the injection of bacteria solution and the subsequent injection of cementing solution (i.e. as applied in the traditional two-phase MICP soil improvement), an injection of leaching solution with an ionic strength lower than the bacteria solution could cause partial bacteria detachment near the injection zone (Choi et al. 2017), thus potentially mitigating the non-uniformity of bacteria deposition (i.e. more deposition near injection zones).

Challenge 2 Optimization of treatment fluids

A critical aspect in the up-scaling of MICP treatment is the optimization of treatment fluid in order to minimise both cost and carbon footprint of treatment and to achieve a better cementation efficiency. An ability to quantify and predict the transport of *S. pasteurii*, under varying physical and chemical conditions, will enable optimization of the injection strategy. For example, we have shown that using 0.48 OD₆₀₀ bacteria results in a higher retention efficiency of *S. pasteurii* compared to 1.0 OD₆₀₀. The injection of bacteria solution with higher ionic strengths (such as 500 and 1000 mM NaCl) also contributes to higher retention efficiency, without inhibiting bacterium survival and effectiveness over the time scale required for a bioaugmentation scheme (refer to SI Figure S2). Lowering the bacterial density and injecting the bacterial solution with a higher IS (e.g. 100 or 500 mM) would enhance the straining efficiency of *S. pasteurii* in a bioaugmentation scheme. The strength of the treated soil depends strongly on the bacteria retained by straining which enhances precipitation at grain-to-grain contacts. Higher straining means a more efficient use of the calcium carbonate and the bacteria, thus potentially reducing the cost and carbon footprint.

Previous studies (Ismail et al. 2002; Tang et al. 2020; Xiao et al. 2019) have proven that the overall cementation efficiency via calcite precipitation is mainly determined by the formation of calcite-bridges between grain contacts. This is closely related to the spatial distribution of the straining cells near grain-to-grain contact points. Our study shows that straining was enhanced from 8.1 to 34.2% when the ionic strength was increased from 0.5 to 500 mM (Fig. 5 and Table 2). In addition, lowering the initial bacteria OD₆₀₀ (from 1.0 to 0.48) caused the straining to increase (from 22.9 to 42.2%), which will also increase the overall cementation efficiency during bioaugmentation treatment.

5 Conclusion

We investigated some key factors influencing the transport and rate of *S. pasteurii* in saturated sand columns such as ionic strength, flow velocity, initial bacteria density, column length, and IS perturbations under injection of 0.5 M CaCl₂ solution and deionised water. The main conclusions are summarised as follows.

Higher ionic strength (from 0.5 to 1000 mM) dramatically enhanced the retention efficiency of *S. pasteurii* through an enhancement of attachment (from 9.4 to 69.6%) and straining (from 8.1 to 34.2%). The enhanced attachment, with increasing IS, is caused by a shift in the interaction energy between bacteria cells and sands from the presence of an energy barrier (0.5 mM) to the appearance of a secondary energy minimum (at 30 and 100 mM) and a primary energy minimum (at 500 and 1000 mM). Increased straining likely results from (1) an increased number of bacteria in the secondary energy minimum (at 30 and 100 mM) prone to be funneled to and retained in small pores formed adjacent to grain–grain junctions, and (2) more straining as a result of the bacterial coagulation of a small number of cells (2–3 cells) that occurs at high ISs (i.e. 500 and 1000 mM). Moreover,

bacterial survival and the effectiveness of urease activity were not influenced by high ionic strengths (up to 1000 mM NaCl) over the timescale required for bioaugmentation.

Experiments using lower flow velocity, lower bacteria density, and a longer column length all correspond to higher bacterial retention. Specifically, increasing the flow velocity (from 50 to 200 cm/h) caused decreasing attachment (from 39.5 to 22.4%) and decreasing straining (from 40.5 to 19.3%) as a result of the increased hydrodynamic shear forces, which tend to reduce the attachment at the secondary minimum and decrease the extent of flow stagnation regions for straining. Lower initial bacteria OD₆₀₀ (from 1.0 to 0.48) enhanced the attachment (from 31.8 to 40.9%) and straining (from 22.9 to 42.2%), respectively, as a result of less site-blockage effects. Shorter column lengths corresponded to a lower retention efficiency, as a result of shorter bacteria residence time. The injection of 0.5 M CaCl₂ solution stabilised the bacterial retention, while the injection with deionised water caused bacterial release.

This study provides clues to guarantee an effective and efficient bacterial delivery into porous media. The two-site kinetic model can reliably quantify and predict bacterial attachment and straining behaviors under the different ionic and hydrodynamic conditions investigated. Our findings can be incorporated into 3D reactive transport models to simulate the MICP process in the field and, ultimately, to optimise the efficiency of bioaugmentation in practical engineering applications.

Supplementary Information The online version contains supplementary material available at <https://doi.org/10.1007/s11242-023-01973-x>.

Acknowledgements This research was supported by the BAM Nuttall/Royal Academy of Engineering Research Chair in *Biomaterial Technologies for Ground Engineering*, Engineering and Physical Sciences Research Council (EPSRC) Capital Award: Emphasising Support for Early Career Researchers (Grant Reference EP/S017917/1). The authors would like to thank Mr. Derek McNee, from Department of Civil and Environmental Engineering—University of Strathclyde (Glasgow), for his contribution to the experimental setups. The authors would also like to thank three anonymous reviewers for giving many constructive comments and invaluable suggestions.

Author Contributions All authors contributed to the study conception and design. Material preparation, data collection and analysis were performed by GS. The first draft of the manuscript was written by GS and all authors commented and edited on previous versions of the manuscript. All authors read and approved the final manuscript.

Funding Royal Academic of Engineering Research Chair, Engineering and Physical Sciences Research Council (EPSRC) Capital Award, EP/S017917/1, James M. Minto

Data Availability The data supporting the analyses and results of this paper are publicly available for download from the following data repository (<https://doi.org/10.15129/82878bbb-d8be-45f6-826e-246fcb1c3530>).

Declarations

Conflict of interest The authors declare no conflicts of interest relevant to this study.

Open Access This article is licensed under a Creative Commons Attribution 4.0 International License, which permits use, sharing, adaptation, distribution and reproduction in any medium or format, as long as you give appropriate credit to the original author(s) and the source, provide a link to the Creative Commons licence, and indicate if changes were made. The images or other third party material in this article are included in the article's Creative Commons licence, unless indicated otherwise in a credit line to the material. If material is not included in the article's Creative Commons licence and your intended use is not permitted by statutory regulation or exceeds the permitted use, you will need to obtain permission directly from the copyright holder. To view a copy of this licence, visit <http://creativecommons.org/licenses/by/4.0/>.

References

- Bai, H., Cochet, N., Pauss, A., Lamy, E.: Bacteria cell properties and grain size impact on bacteria transport and deposition in porous media. *Coll. Surf. B Biointerfaces* **139**, 148–155 (2016). <https://doi.org/10.1016/J.COLSURFB.2015.12.016>
- Barkouki, T.H., Martinez, B.C., Mortensen, B.M., Weathers, T.S., De Jong, J.D., Ginn, T.R., Spycher, N.F., Smith, R.W., Fujita, Y.: Forward and inverse bio-geochemical modeling of microbially induced calcite precipitation in half-meter column experiments. *Transp. Porous Media*. **90**, 23–39 (2011)
- Bradford, S.A., Simunek, J., Bettahar, M., Van Genuchten, M.T., Yates, S.R.: Modeling colloid attachment, straining, and exclusion in saturated porous media. *Environ. Sci. Technol.* **37**, 2242–2250 (2003)
- Bradford, S.A., Simunek, J., Bettahar, M., Tadassa, Y.F., Van Genuchten, M.T., Yates, S.R.: Straining of colloids at textural interfaces. *Water Resour. Res.* **41**, 10404 (2005). <https://doi.org/10.1029/2004WR003675>
- Bradford, S.A., Torkzaban, S., Walker, S.L.: Coupling of physical and chemical mechanisms of colloid straining in saturated porous media. *Water Res.* **41**, 3012–3024 (2007). <https://doi.org/10.1016/J.WATRES.2007.03.030>
- Bradford, S.A., Morales, V.L., Zhang, W., Harvey, R.W., Packman, A.I., Mohanram, A., Welty, C.: Transport and fate of microbial pathogens in agricultural settings. *Crit. Rev. Environ. Sci. Technol.* **43**, 775–893 (2013). <https://doi.org/10.1080/10643389.2012.710449>
- Bradford, S.A., Yates, S.R., Bettahar, M., Simunek, J.: Physical factors affecting the transport and fate of colloids in saturated porous media. *Water Resour. Res.* **38**, 63-1–63-12 (2002). <https://doi.org/10.1029/2002wr001340>
- Bradford, S.A., Simunek, J., Walker, S.L.: Transport and straining of *E. coli* O157:H7 in saturated porous media. *Water Resour. Res.* (2006). <https://doi.org/10.1029/2005WR004805>
- Burbank, M., Weaver, T., Lewis, R., Williams, T., Williams, B., Crawford, R.: Geotechnical tests of sands following bioinduced calcite precipitation catalyzed by indigenous bacteria. *J. Geotech. Geoenviron. Eng.* **139**, 928–936 (2013). [https://doi.org/10.1061/\(ASCE\)GT.1943-5606.0000781](https://doi.org/10.1061/(ASCE)GT.1943-5606.0000781)
- Camesano, T.A., Logan, B.E.: Influence of fluid velocity and cell concentration on the transport of motile and nonmotile bacteria in porous media. *Environ. Sci. Technol.* **32**, 1699–1708 (1998). <https://doi.org/10.1021/es970996m>
- Choi, N.C., Kim, D.J., Kim, S.B.: Quantification of bacterial mass recovery as a function of pore-water velocity and ionic strength. *Res. Microbiol.* **158**, 70–78 (2007). <https://doi.org/10.1016/j.resmic.2006.09.007>
- Choi, N.-C., Choi, J.-W., Kwon, K.-S., Lee, S.-G., Lee, S.: Quantifying bacterial attachment and detachment using leaching solutions of various ionic strengths after bacterial pulse. *AMB Express* **71**(7), 1–9 (2017). <https://doi.org/10.1186/S13568-017-0340-2>
- Creppy, A., Clément, E., Douarche, C., D'Angelo, M.V., Auradou, H.: Effect of motility on the transport of bacteria populations through a porous medium. *Phys. Rev. Fluids*. **4**, 013102 (2019). <https://doi.org/10.1103/PHYSREVFLUIDS.4.013102/FIGURES/10/MEDIUM>
- Cuthbert, M.O., McMillan, L.A., Handley-Sidhu, S., Riley, M.S., Tobler, D.J., Phoenix, V.R.: A field and modeling study of fractured rock permeability reduction using microbially induced calcite precipitation. *Environ. Sci. Technol.* **47**, 13637–13643 (2013). <https://doi.org/10.1021/es402601g>
- DeJong, J.T., Mortensen, B.M., Martinez, B.C., Nelson, D.C.: Bio-mediated soil improvement. *Ecol. Eng.* **36**, 197–210 (2010). <https://doi.org/10.1016/j.ecoleng.2008.12.029>
- El Mountassir, G., Lunn, R.J., Moir, H., MacLachlan, E.: Hydrodynamic coupling in microbially mediated fracture mineralization: Formation of self-organized groundwater flow channels. *Water Resour. Res.* **50**, 1–16 (2014). <https://doi.org/10.1002/2013WR013578>
- El Mountassir, G., Minto, J.M., van Paassen, L.A., Salifu, E., Lunn, R.J.: Applications of Microbial Processes in Geotechnical Engineering. *Adv. Appl. Microbiol.* **104**, 39–91 (2018). <https://doi.org/10.1016/BS.AAMBS.2018.05.001>
- Foppen, J.W., van Herwerden, M., Schijven, J.: Measuring and modelling straining of *Escherichia coli* in saturated porous media. *J. Contam. Hydrol.* **93**, 236–254 (2007). <https://doi.org/10.1016/J.JCONHYD.2007.03.001>
- Fujita, Y., Taylor, J.L., Gresham, T.L.T., Delwiche, M.E., Colwell, F.S., McLing, T.L., Petzke, L.M., Smith, R.W.: Stimulation of microbial urea hydrolysis in groundwater to enhance calcite precipitation. *Environ. Sci. Technol.* **42**, 3025–3032 (2008). <https://doi.org/10.1021/ES702643G>
- Gargiulo, G., Bradford, S., Šimunek, J., Ustohal, P., Vereecken, H., Klumpp, E.: Bacteria transport and deposition under unsaturated conditions: the role of the matrix grain size and the bacteria surface protein. *J. Contam. Hydrol.* **92**, 255–273 (2007). <https://doi.org/10.1016/J.JCONHYD.2007.01.009>

- Gargiulo, G., Bradford, S.A., Simunek, J., Ustohal, P., Vereecken, H., Klumpp, E.: bacteria transport and deposition under unsaturated flow conditions: the role of water content and bacteria surface hydrophobicity. *Vadose Zo. J.* **7**, 406–419 (2008). <https://doi.org/10.2136/VZJ2007.0068>
- Gomez, M.G., Anderson, C.M., Graddy, C.M.R., DeJong, J.T., Nelson, D.C., Ginn, T.R.: Large-scale comparison of bioaugmentation and biostimulation approaches for biocementation of sands. *J. Geotech. Geoenvironmental Eng.* **143**, 04016124 (2017). [https://doi.org/10.1061/\(ASCE\)GT.1943-5606.0001640](https://doi.org/10.1061/(ASCE)GT.1943-5606.0001640)
- Gomez, M.G., Martinez, B.C., DeJong, J.T., Hunt, C.E., deVlaming, L.A., Major, D.W., Dworatzek, S.M.: Field-scale bio-cementation tests to improve sands. *Proc. Inst. Civ. Eng. - Gr. Improv.* **168**, 206–216 (2015). <https://doi.org/10.1680/grim.13.00052>
- Hahn, M.W., Dean, A., O'Melia, C.R.: Aquasols: on the role of secondary minima†. *Environ. Sci. Technol.* **38**, 5915–5924 (2004). <https://doi.org/10.1021/ES049746D>
- Harvey, R.W., Metge, D.W., Barber, L.B., Aiken, G.R.: Effects of altered groundwater chemistry upon the pH-dependency and magnitude of bacterial attachment during transport within an organically contaminated sandy aquifer. *Water Res.* **44**, 1062–1071 (2010). <https://doi.org/10.1016/j.watres.2009.09.008>
- Hendry, M.J., Lawence, J.R., Maloszewski, P.: Effects of velocity on the transport of two bacteria through saturated sand. *Ground Water* **37**, 103 (1999)
- Hogg, R., Healy, T.W., Fuerstenau, D.: Mutual coagulation of colloidal dispersions. *Trans. Faraday Soc.* **62**, 1638–1651 (1966). <https://doi.org/10.1039/TF9666201638>
- Hommel, J., Lauchnor, E., Gerlach, R., Cunningham, A.B., Ebigbo, A., Helmig, R., Class, H.: Investigating the influence of the initial biomass distribution and injection strategies on biofilm-mediated calcite precipitation in porous media. *Transp. Porous Media.* **114**, 557–579 (2016)
- Ismail, M.A., Joer, H.A., Randolph, M.F., Meritt, A.: Cementation of porous materials using calcite. *Geotechnique* **52**, 313–324 (2002). <https://doi.org/10.1680/GEOT.2002.52.5.313/ASSET/IMAGES/SMALL/GEOT52-313-F20.GIF>
- Jain, S., Arnepalli, D.N.: Adhesion and deadhesion of ureolytic bacteria on sand under variable pore fluid chemistry. *J. Environ. Eng.* **146**, 04020038 (2020). [https://doi.org/10.1061/\(ASCE\)EE.1943-7870.0001708](https://doi.org/10.1061/(ASCE)EE.1943-7870.0001708)
- Jiang, N.J., Wang, Y.J., Chu, J., Kawasaki, S., Tang, C.S., Cheng, L., Du, Y.J., Shashank, B.S., Singh, D.N., Han, X.L., Wang, Y.Z.: Bio-mediated soil improvement: an introspection into processes, materials, characterization and applications. *Soil Use Manag.* **38**, 68–93 (2022). <https://doi.org/10.1111/SUM.12736>
- Kinoshita, T., Bales, R.C., Yahya, M.T., Gerba, C.P.: Bacteria transport in a porous medium: retention of bacillus and pseudomonas on silica surfaces. *Water Res.* **27**, 1295–1301 (1993). [https://doi.org/10.1016/0043-1354\(93\)90216-5](https://doi.org/10.1016/0043-1354(93)90216-5)
- Kwak, E., Kim, J.H., Choi, J.W., Lee, S.: Injection strategy for effective bacterial delivery in bioaugmentation scheme by controlling ionic strength and pore-water velocity. *J. Environ. Manage.* **328**, 116971 (2023). <https://doi.org/10.1016/J.JENVMAN.2022.116971>
- Lauchnor, E.G., Schultz, L.N., Bugni, S., Mitchell, A.C., Cunningham, A.B., Gerlach, R.: Bacterially induced calcium carbonate precipitation and strontium coprecipitation in a porous media flow system. *Environ. Sci. Technol.* **47**, 1557–1564 (2013)
- Li, K., Ma, H.: Deposition dynamics of rod-shaped colloids during transport in porous media under favorable conditions. *Langmuir* **34**, 2967–2980 (2018). https://doi.org/10.1021/ACS.LANGMUIR.7B03983/ASSET/IMAGES/MEDIUM/LA-2017-03983A_M022.GIF
- Liao, S., Ghosh, A., Becker, M.D., Abriola, L.M., Cápiro, N.L., Fortner, J.D., Pennell, K.D.: Effect of rhamnolipid biosurfactant on transport and retention of iron oxide nanoparticles in water-saturated quartz sand. *Environ. Sci. Nano.* **8**, 311–327 (2021). <https://doi.org/10.1039/D0EN01033B>
- Liu, J., Ford, R.M., Smith, J.A.: Idling time of motile bacteria contributes to retardation and dispersion in sand porous medium. *Environ. Sci. Technol.* **45**, 3945–3951 (2011). <https://doi.org/10.1021/es104041t>
- Martinez, B.C., DeJong, J.T., Ginn, T.R., Montoya, B.M., Barkouki, T.H., Hunt, C., Tanyu, B., Major, D.: Experimental optimization of microbial-induced carbonate precipitation for soil improvement. *J. Geotech. Geoenvironmental Eng.* **139**, 587–598 (2013). [https://doi.org/10.1061/\(ASCE\)GT.1943-5606.0000787](https://doi.org/10.1061/(ASCE)GT.1943-5606.0000787)
- McCaulou, D.R., Bales, R.C., Arnold, R.G.: Effect of temperature-controlled motility on transport of bacteria and microspheres through saturated sediment. *Water Resour. Res.* **31**, 271–280 (1995). <https://doi.org/10.1029/94WR02569>
- McDowell-Boyer, L.M., Hunt, J.R., Sitar, N.: Particle transport through porous media. *Water Resour. Res.* **22**, 1901–1921 (1986). <https://doi.org/10.1029/WR022i013p01901>


- Minto, J.M., MacLachlan, E., El Mountassir, G., Lunn, R.J.: Rock fracture grouting with microbially induced carbonate precipitation. *Water Resour. Res.* **52**, 8827–8844 (2016). <https://doi.org/10.1002/2016WR018884>
- Minto, J.M., Hingerl, F.F., Benson, S.M., Lunn, R.J.: X-ray CT and multiphase flow characterization of a ‘bio-grouted’ sandstone core: the effect of dissolution on seal longevity. *Int. J. Greenh. Gas Control.* **64**, 152–162 (2017). <https://doi.org/10.1016/j.ijggc.2017.07.007>
- Minto, J.M., Tan, Q., Lunn, R.J., El Mountassir, G., Guo, H., Cheng, X.: ‘Microbial mortar’-restoration of degraded marble structures with microbially induced carbonate precipitation. *Constr. Build. Mater.* **180**, 44–54 (2018). <https://doi.org/10.1016/j.conbuildmat.2018.05.200>
- Minto, J.M., Lunn, R.J., El Mountassir, G.: Development of a reactive transport model for field-scale simulation of microbially induced carbonate precipitation. *Water Resour. Res.* **55**, 7229–7245 (2019)
- Mitchell, A.C., Dideriksen, K., Spangler, L.H., Cunningham, A.B., Gerlach, R.: Microbially enhanced carbon capture and storage by mineral-trapping and solubility-trapping. *Environ. Sci. Technol.* **44**, 5270–5276 (2010). <https://doi.org/10.1021/ES903270W>
- Nassar, M.K., Gurung, D., Bastani, M., Ginn, T.R., Shafei, B., Gomez, M.G., Graddy, C.M.R., Nelson, D.C., DeJong, J.T.: Large-scale experiments in microbially induced calcite precipitation (MICP): reactive transport model development and prediction. *Water Resour. Res.* **54**, 480–500 (2018). <https://doi.org/10.1002/2017WR021488>
- Phillips, A.J., Lauchnor, E., Eldring, J., Esposito, R., Mitchell, A.C., Gerlach, R., Cunningham, A.B., Spangler, L.H.: Potential CO₂ leakage reduction through biofilm-induced calcium carbonate precipitation. *Environ. Sci. Technol.* **47**, 142–149 (2013). <https://doi.org/10.1021/es301294q>
- Phillips, A.J., Cunningham, A.B., Gerlach, R., Hiebert, R., Hwang, C., Lomans, B.P., Westrich, J., Mantilla, C., Kirksey, J., Esposito, R., Spangler, L.: Fracture sealing with microbially-induced calcium carbonate precipitation: a field study. *Environ. Sci. Technol.* **50**, 4111–4117 (2016). <https://doi.org/10.1021/acs.est.5b05559>
- Ramachandran, S.K., Ramakrishnan, V., Bang, S.S.: Remediation of concrete using micro-organisms. *ACI Mater. Journal-American Concr. Inst.* **98**, 3–9 (2001)
- Redman, J.A., Walker, S.L., Elimelech, M.: Bacterial adhesion and transport in porous media: role of the secondary energy minimum. *Environ. Sci. Technol.* **38**, 1777–1785 (2004). <https://doi.org/10.1021/es0348871>
- Rijnaarts, H.H.M., Norde, W., Bouwer, E.J., Lyklema, J., Zehnder, A.J.B.: Bacterial deposition in porous media: effects of cell-coating, substratum hydrophobicity, and electrolyte concentration. *Environ. Sci. Technol.* **30**, 2877–2883 (1996). <https://doi.org/10.1021/ES9605984/ASSET/IMAGES/LARGE/ES9605984F00008.JPEG>
- Salifu, E., MacLachlan, E., Iyer, K.R., Knapp, C.W., Tarantino, A.: Application of microbially induced calcite precipitation in erosion mitigation and stabilisation of sandy soil foreshore slopes: a preliminary investigation. *Eng. Geol.* **201**, 96–105 (2016). <https://doi.org/10.1016/J.ENGGE0.2015.12.027>
- Sang, W., Morales, V.L., Zhang, W., Stoof, C.R., Gao, B., Schatz, A.L., Zhang, Y., Steenhuis, T.S.: Quantification of colloid retention and release by straining and energy minima in variably saturated porous media. *Environ. Sci. Technol.* **47**, 8256–8264 (2013). <https://doi.org/10.1021/es400288c>
- Sasidharan, S., Torkzaban, S., Bradford, S.A., Dillon, P.J., Cook, P.G.: Coupled effects of hydrodynamic and solution chemistry on long-term nanoparticle transport and deposition in saturated porous media. *Coll. Surf. A Physicochem. Eng. Asp.* **457**, 169–179 (2014). <https://doi.org/10.1016/J.COLSURFA.2014.05.075>
- Seymour, M.B., Chen, G., Su, C., Li, Y.: Transport and retention of colloids in porous media: does shape really matter? *Environ. Sci. Technol.* **47**, 8391–8398 (2013). https://doi.org/10.1021/ES4016124/SUPPL_FILE/ES4016124_SI_001.PDF
- Shellenberger, K., Logan, B.E.: Effect of molecular scale roughness of glass beads on colloidal and bacterial deposition. *Environ. Sci. Technol.* **36**, 184–189 (2002). <https://doi.org/10.1021/ES015515K/ASSET/IMAGES/LARGE/ES015515KF00007.JPEG>
- Šimunek, J., Van Genuchten, M.T., Sejna, M.: The HYDRUS-1D software package for simulating the one-dimensional movement of water, heat, and multiple solutes in variably-saturated media. *Univ. California-Riverside Res. Reports.* **3**, 1–240 (2005)
- Šimunek, J., Šejna, M., Van Genuchten, M.T.: The HYDRUS-2D software package for simulating the two-dimensional movement of water, heat, and multiple solutes in variably-saturated media: Version 2.0. US Salinity Laboratory, Agricultural Research Service, US Department of Agriculture (1999)
- Šimunek, J.S., He, C., Pang, L., Bradford, S.A.: Colloid-facilitated solute transport in variably saturated porous medianumerical model and experimental verification. *Vadose Zo. J.* **5**, 1035–1047 (2006). <https://doi.org/10.2136/VZJ2005.0151>

- Steinacher, F.: The Potential for Microbially Induced Carbonate Precipitation to Support Wellbore Sealing and Zonal Isolation in the Hydrocarbon Industry, (2021)
- Stocks-Fischer, S., Galinat, J.K., Bang, S.S.: Microbiological precipitation of CaCO₃. *Soil Biol. Biochem.* **31**, 1563–1571 (1999). [https://doi.org/10.1016/S0038-0717\(99\)00082-6](https://doi.org/10.1016/S0038-0717(99)00082-6)
- Stumpp, C., Lawrence, J.R., Hendry, M.J., Maloszewski, P.: Transport and bacterial interactions of three bacterial strains in saturated column experiments. *Environ. Sci. Technol.* **45**, 2116–2123 (2011). <https://doi.org/10.1021/es103569u>
- Tan, Y., Gannon, J.T., Baveye, P., Alexander, M.: Transport of bacteria in an aquifer sand: experiments and model simulations. *Water Resour. Res.* **30**, 3243–3252 (1994). <https://doi.org/10.1029/94WR02032>
- Tang, C.S., Yin, L.Y., Jiang, N.J., Zhu, C., Zeng, H., Li, H., Shi, B.: Factors affecting the performance of microbial-induced carbonate precipitation (MICP) treated soil: a review. *Environ. Earth Sci.* **79**, 1–23 (2020). <https://doi.org/10.1007/S12665-020-8840-9/FIGURES/24>
- Tobler, D.J., Maclachlan, E., Phoenix, V.R.: Microbially mediated plugging of porous media and the impact of differing injection strategies. *Ecol. Eng.* **42**, 270–278 (2012)
- Tobler, D.J., Cuthbert, M.O., Phoenix, V.R.: Transport of *Sporosarcina pasteurii* in sandstone and its significance for subsurface engineering technologies. *Appl. Geochemistry.* **42**, 38–44 (2014). <https://doi.org/10.1016/j.apgeochem.2014.01.004>
- Tobler, D.J., Minto, J.M., El Mountassir, G., Lunn, R.J., Phoenix, V.R.: Microscale analysis of fractured rock sealed with microbially induced CaCO₃ precipitation: influence on hydraulic and mechanical performance. *Water Resour. Res.* **54**, 8295–8308 (2018)
- Torkzaban, S., Bradford, S.A., van Genuchten, M.T., Walker, S.L.: Colloid transport in unsaturated porous media: the role of water content and ionic strength on particle straining. *J. Contam. Hydrol.* **96**, 113–127 (2008a). <https://doi.org/10.1016/J.JCONHYD.2007.10.006>
- Torkzaban, S., Tazehkand, S.S., Walker, S.L., Bradford, S.A.: Transport and fate of bacteria in porous media: coupled effects of chemical conditions and pore space geometry. *Water Resour. Res.* (2008b). <https://doi.org/10.1029/2007WR006541>
- van Paassen, L.A., Ghose, R., van der Linden, T.J.M., van der Star, W.R.L., van Loosdrecht, M.C.M.: Quantifying biomediated ground improvement by ureolysis: large-scale biogROUT experiment. *J. Geotech. Geoenvironmental Eng.* **136**, 1721–1728 (2010). [https://doi.org/10.1061/\(ASCE\)GT.1943-5606.0000382](https://doi.org/10.1061/(ASCE)GT.1943-5606.0000382)
- van Wijngaarden, W.K., Vermolen, F.J., van Meurs, G.A.M., Vuik, C.: Modelling biogROUT: a new ground improvement method based on microbial-induced carbonate precipitation. *Transp. Porous Media.* **87**, 397–420 (2011)
- van Wijngaarden, W.K., van Paassen, L.A., Vermolen, F.J., van Meurs, G.A.M., Vuik, C.: Simulation of front instabilities in density-driven flow, using a reactive transport model for biogROUT combined with a randomly distributed permeability field. *Transp. Porous Media.* **112**, 333–359 (2016)
- Vasiliadou, I.A., Chrysikopoulos, C.V.: Cotransport of *Pseudomonas putida* and kaolinite particles through water-saturated columns packed with glass beads. *Water Resour. Res.* **47**, 2543 (2011). <https://doi.org/10.1029/2010WR009560>
- Walker, S.L., Redman, J.A., Elimelech, M.: Role of cell surface lipopolysaccharides in *Escherichia coli* K12 adhesion and transport. *Langmuir* **20**, 7736–7746 (2004). <https://doi.org/10.1021/LA049511F/ASSET/IMAGES/LARGE/LA049511FF00009.JPEG>
- Walker, S.L., Redman, J.A., Elimelech, M.: Influence of growth phase on bacterial deposition: Interaction mechanisms in packed-bed column and radial stagnation point flow systems. *Environ. Sci. Technol.* **39**, 6405–6411 (2005). <https://doi.org/10.1021/ES050077T/ASSET/IMAGES/LARGE/ES050077TF00004.JPEG>
- Weiss, T.H., Mills, A.L., Hornberger, G.M., Herman, J.S.: Effect of bacterial cell shape on transport of bacteria in porous media. *Environ. Sci. Technol.* **29**, 1737–1740 (1995)
- Whiffin, V.S., van Paassen, L.A., Harkes, M.P.: Microbial carbonate precipitation as a soil improvement technique. *Geomicrobiol. J.* **24**, 417–423 (2007). <https://doi.org/10.1080/01490450701436505>
- Xiao, Y., Stuedlein, A.W., Ran, J., Evans, T.M., Cheng, L., Liu, H., van Paassen, L.A., Chu, J.: Effect of particle shape on strength and stiffness of biocemented glass beads. *J. Geotech. Geoenvironmental Eng.* **145**, 06019016 (2019). [https://doi.org/10.1061/\(ASCE\)GT.1943-5606.0002165](https://doi.org/10.1061/(ASCE)GT.1943-5606.0002165)
- Xu, S., Saiers, J.E.: Colloid straining within water-saturated porous media: effects of colloid size nonuniformity. *Water Resour. Res.* **45**, 5501 (2009). <https://doi.org/10.1029/2008WR007258>
- Xu, S., Gao, B., Saiers, J.E.: Straining of colloidal particles in saturated porous media. *Water Resour. Res.* **42**, 12–16 (2006). <https://doi.org/10.1029/2006WR004948>
- Yang, Y., Chu, J., Liu, H., Cheng, L.: Improvement of uniformity of biocemented sand column using CH₃COOH-buffered one-phase-low-pH injection method. *Acta Geotech.* **18**, 413–428 (2022). <https://doi.org/10.1007/S11440-022-01576-8/FIGURES/17>

Yao, K.-M., Habibian, M.T., O'melia, C.R.: Water and waste water filtration: concepts and applications. *Environ. Sci. Technol.* **5**, 1105–1112 (1971)

Publisher's Note Springer Nature remains neutral with regard to jurisdictional claims in published maps and institutional affiliations.

Authors and Affiliations

Guijie Sang¹  · Rebecca J. Lunn¹ · Grainne El Mountassir¹ · James M. Minto¹

✉ Guijie Sang
guijie.sang@strath.ac.uk

¹ Department of Civil and Environmental Engineering, University of Strathclyde, Glasgow, UK